Sensors and Materials, Vol. 37, No. 8 (2025) 3419–3429
MYU Tokyo

S & M 4126

Enhanced Green Emission in Solid-state-synthesized LaF_3–LaOF:Yb^{3+}/Tb^{3+} Upconversion Phosphors

Toshihiro Nonaka,[1*] Mutsuto Yamamoto,[2] Takahito Imai,[3] and Shin-Ichi Yamamoto[4]

[1]Department of Electrical and Electronic Engineering, Faculty of Science and Engineering, Otemon Gakuin University, 2-1-15 Nishiai, Ibaraki City, Osaka 567-8502, Japan
[2]Department of Electrical and Electronic Engineering, National Institute of Technology, Toyota College, 2-1 Eiseicho, Toyota, Aichi 471-8525, Japan
[3]Materials Chemistry Course, Faculty of Advanced Science and Technology, Ryukoku University, 1-5 Yokotani, Oe-cho, Seta, Ohtsu City, Shiga 520-2194, Japan
[4]Electronics, Information, and Communication Engineering Course, Faculty of Advanced Science and Technology, Ryukoku University, 1-5 Yokotani, Oe-cho, Seta, Ohtsu City, Shiga 520-2194, Japan

(Received June 6, 2025; accepted July 10, 2025)

Keywords: upconversion, LaF_3, LaOF, Yb^{3+}, Tb^{3+}

In this study, LaF_3–LaOF:Yb^{3+}/Tb^{3+} was synthesized by a solid-state reaction method, and the effects of varying molar ratios on the crystal structure and optical properties of the resulting material were analyzed. Crystal structure analysis using X-ray diffraction revealed that the synthesized samples were composed of LaOF and LaF_3. The photoluminescence (PL) spectra showed peaks at 486 ($^5D_4 \rightarrow {}^7F_6$), 541 ($^5D_4 \rightarrow {}^7F_5$), 583 ($^5D_4 \rightarrow {}^7F_4$), and 620 nm ($^5D_4 \rightarrow {}^7F_3$). The analysis of the pump-power dependence of the PL intensity revealed that the emission was a two-photon process, because the slopes obtained at wavelengths of 486 and 541 nm were approximately equivalent to 2. These research findings contribute to the further development of Tb^{3+}-doped phosphors for temperature-sensing applications.

1. Introduction

Upconversion (UC) technology, which is used to convert near-infrared (NIR) electromagnetic waves into visible light, has recently attracted considerable attention.[1] UC gained widespread recognition in 1966 when Auzel reported the occurrence of energy transfer between two rare-earth ions.[2,3] UC phosphors have been applied in bioimaging,[4,5] photocatalysis,[6,7] fingerprint analysis,[8] and temperature sensing.[9,10] Notably, in 2024, Li *et al.* demonstrated the particle-size-dependent energy transfer effect of lanthanides, which enhanced the UC quantum yield to 13.0% ± 1.3%.[11]

$NaYF_4$ is a commonly used host material for UC phosphors.[12,13] To improve the luminescence efficiency of UC phosphors, nonradiative losses must be minimized; therefore, low-phonon-energy fluorides are generally used as host materials.[10] In this study, a LaF_3–LaOF composite was used as the host material. Because the ionic radii and valences of La^{3+} are similar to those of rare-earth elements, doping with these elements does not induce significant crystal

*Corresponding author: e-mail: t-nonaka@otemon.ac.jp
https://doi.org/10.18494/SAM5773

ISSN 0914-4935
https://myukk.org/

lattice distortion.[14,15] Upon heating, a portion of LaF_3 undergoes oxidation, forming the LaF_3–LaOF composite. Our research group has demonstrated that the formation of LaF_3–LaOF composites enhances the photoluminescence (PL) intensity more effectively than the complete transformation of LaF_3 to LaOF.[16] Furthermore, the LaF_3–LaOF composite demonstrated chemical stability, and the fluorescence intensity ratio of its UC luminescence was reproducible across a range of temperatures.[17]

Common dopant combinations for UC phosphors include Yb–Er, Yb–Ho, and Yb–Tm.[4,9] The Yb–Tb combination was used in this study. The luminescence of Yb–Tb originates from cooperative energy transfer, typically associated with relatively low luminescence efficiency, which is a major disadvantage. Nevertheless, Tb^{3+} has spectral characteristics different from those of Er^{3+}, Ho^{3+}, and Tm^{3+}, rendering it useful for achieving luminescence at specific emission wavelengths. The luminescence of Tb^{3+} arises from electronic transitions within its 4f orbitals, typically characterized by a green emission with a sharp spectral profile. Furthermore, research into the use of Tb^{3+} as a phosphor material for LEDs is ongoing.[18]

In this study, LaF_3–LaOF:Yb^{3+}/Tb^{3+} is synthesized by a solid-state reaction method, and the effects of varying molar ratios on the crystal structure and optical properties of the synthesized material are analyzed. In this study, we aim to elucidate the luminescence mechanism of LaF_3–LaOF:Yb^{3+}/Tb^{3+}. Although the Yb^{3+} and Tb^{3+} doping of LaF_3 has been reported,[19,20] the luminescence properties of the LaF_3–LaOF composite doped with these UC phosphors via the solid-state reaction method have not yet been explored. Furthermore, Tb^{3+}-doped downconversion phosphors can serve as temperature sensors.[21] In this study, we analyze the optical properties of LaF_3–LaOF:Yb^{3+}/Tb^{3+} with the aim of utilizing them for temperature-sensing applications.

2. Experimental Conditions

Samples were synthesized by a solid-state reaction method. LaF_3 (99.9%), Yb_2O_3 (99.9%), and Tb_2O_3 (99.9%) powders were obtained from Kojundo Chemical Lab. Co., Ltd. and mixed at a La:Yb:Tb molar ratio of 1:x:y (x = 0.02–0.10 and y = 0.08–0.12). The mixed powder was subsequently pressed into a cylinder measuring 15 mm in diameter and 3 mm in height. The formed samples were placed in alumina crucibles and fired in an electric furnace. During firing, the temperature inside the electric furnace was increased from room temperature to 1150 °C over a period of 2 h and was subsequently maintained at 1150 °C for 1 h. Thereafter, the samples were spontaneously cooled from 1150 °C to room temperature.

The synthesized materials were evaluated in terms of reflectance, crystal structure, elemental mapping, PL characteristics, and the pump-power dependence of PL intensity. For the reflectance measurements, a halogen light source (HL-2000-LL; Ocean Insight), a diffuse reflectance standard (WS-1; Ocean Insight), and a standard reflectance measurement probe (R400-7-VIS-NIR; Ocean Insight) were used. Light from the standard reflectance measurement probe was directed at the sample at an angle of 45°, and a portion of diffuse reflection was measured. The crystal structure was analyzed via X-ray diffraction (XRD; Ultima IV, Rigaku Holdings Corporation). For the elemental mapping analysis, the milled samples were embedded in resin,

and the cross sections of the samples were prepared using a cross-section polisher. Subsequently, the cross-sectional geometry and elemental mapping of the samples were analyzed. Furthermore, a multibeam system (JIB-4601F; JEOL) equipped with a scanning electron microscope (SEM) and energy dispersive X-ray spectroscopy (EDS) equipment (X-MAX, Oxford) was used for sample characterization. An NIR laser featuring a wavelength of 980 nm and power of 200 mW was used as the excitation light source for PL analysis. In the analysis of the pump-power dependence of the PL intensity, neutral density (ND) filters were used to control the power of the excitation source. ND filters with transmittances of 78.5, 56.2, and 40.8% at 980 nm were positioned in front of the excitation laser source (200 mW), yielding excitation powers of 157, 112, and 82 mW, respectively. The reflectance, PL, and pump-power dependence analyses were all conducted using the OCEAN SR spectrometer (Ocean Insight).

3. Results and Discussion

The reflection spectrum of LaF_3–LaOF:Yb^{3+}/Tb^{3+}, with a La:Yb:Tb molar ratio of 1:0.06:0.10, is plotted in Fig. 1. A decrease in the reflectance is observed at approximately 950 nm. This absorption peak at approximately 950 nm is considered to originate from the Yb^{3+} transition from $^2F_{7/2}$ to $^2F_{5/2}$.[22] Furthermore, the reflectance at approximately 950 nm decreases with increasing Yb^{3+} doping concentration. The energy band diagram of Tb^{3+} depicts an absorption peak at 486 nm; however, no clear absorption peak is observed in Fig. 1.

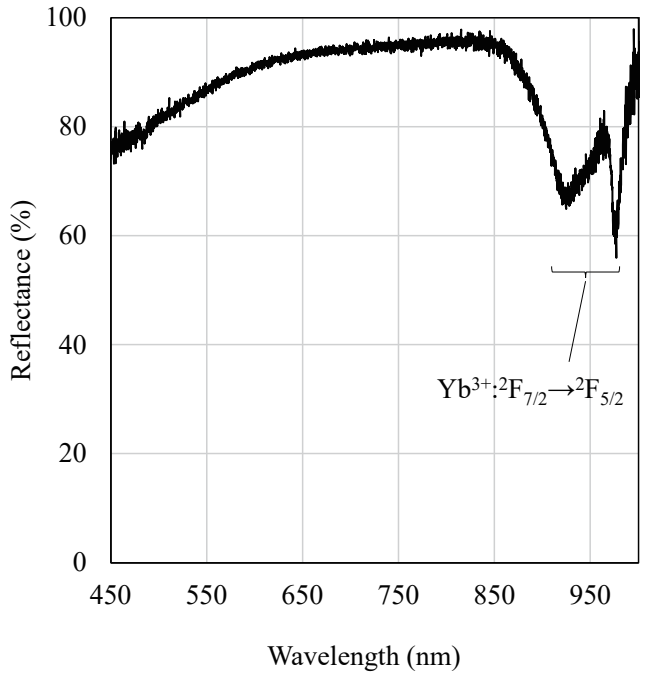

Fig. 1. Reflection spectrum of LaF_3–LaOF:Yb^{3+}/Tb^{3+} with a La:Yb:Tb molar ratio of 1:0.06:0.10.

The results of the crystal structure analysis are presented in Fig. 2. Figures 2(a) and 2(b) depict the XRD patterns of LaF_3–LaOF:Yb^{3+}/Tb^{3+} possessing a La:Yb:Tb molar ratio of 1:x:0.10 (x = 0.02–0.10) and the dependence of the LaF_3 and LaOF volumes on the Yb^{3+} concentration, respectively. Figures 2(c) and 2(d) illustrate the XRD patterns of LaF_3–LaOF:Yb^{3+}/Tb^{3+} possessing a La:Yb:Tb molar ratio of 1:0.06:y (y = 0.08–0.12) and the dependence of the LaF_3

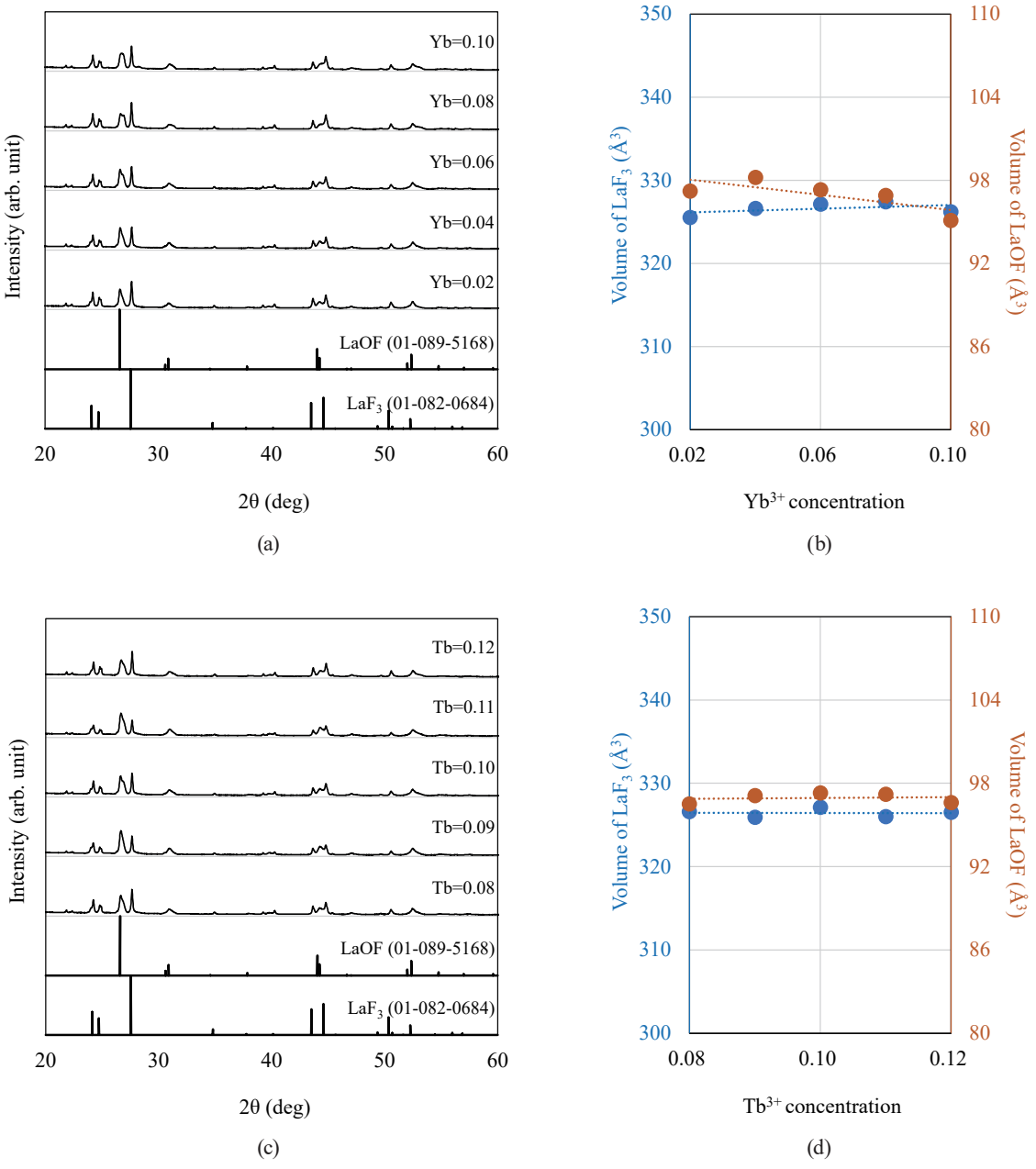

Fig. 2. (Color online) Results of crystal structure analysis. (a) XRD patterns of LaF_3–LaOF:Yb^{3+}/Tb^{3+} possessing a La:Yb:Tb molar ratio of 1:x:0.10 (x = 0.02–0.10) and (b) dependence of volume on Yb^{3+} concentration. (c) XRD patterns of LaF_3–LaOF:Yb^{3+}/Tb^{3+} possessing a La:Yb:Tb molar ratio of 1:0.06:y (y = 0.08–0.12) and (d) dependence of volume on Tb^{3+} concentration.

and LaOF volumes on the Tb^{3+} concentration, respectively. The lattice constants and volumes were calculated by the least squares method using the PDXL2 software from Rigaku Holdings Corporation. The XRD patterns of LaOF (01-089-5168) and LaF_3 (01-082-0684) obtained from the Inorganic Crystal Structure Database (ICSD) are presented in the lower parts of Figs. 2(a) and 2(c), which confirm that all the synthesized samples are composed of LaOF and LaF_3. Figure 2(b) reveals that the LaOF and LaF_3 volumes are 95.1–98.2 and 325.5–227.4 $Å^3$, respectively. As presented in Fig. 2(d), the LaOF and LaF_3 volumes are 96.5–97.3 and 325.9–327.1 $Å^3$, respectively.

The lattice constants of LaOF in LaF_3–$LaOF:Yb^{3+}/Tb^{3+}$ possessing a La:Yb:Tb molar ratio of 1:0.06:0.10 are a = 4.089 Å, c = 5.820 Å, and V = 97.3 $Å^3$. The LaOF volume (01-089-5168) obtained from ICSD is 97.673 $Å^3$. Therefore, the volume of the synthesized sample is 0.3% less than that recorded in ICSD. The lattice constants of LaF_3 in the LaF_3–$LaOF:Yb^{3+}/Tb^{3+}$ sample possessing a La:Yb:Tb molar ratio of 1:0.06:0.10 are a = 7.174 Å, c = 7.337 Å, and V = 327.1 $Å^3$. The LaF_3 volume (01-082-0684) listed in ICSD is 331.144 $Å^3$. Therefore, the volume of the synthesized sample is 1.2% less than that recorded in ICSD. The ionic radii of Yb^{3+}, Tb^{3+}, and La^{3+}, all of which have coordination number = 8, are 0.985, 1.040, and 1.160 Å, respectively.[23] The substitution of Yb^{3+} or Tb^{3+} for La^{3+} may have reduced the volumes of LaOF and LaF_3 synthesized in this study compared with those provided in ICSD.

The SEM and EDS analysis results obtained for LaF_3–$LaOF:Yb^{3+}/Tb^{3+}$, with a La:Yb:Tb molar ratio of 1:0.06:0.10, are presented in Fig. 3. Figure 3(a) depicts the cross-sectional SEM

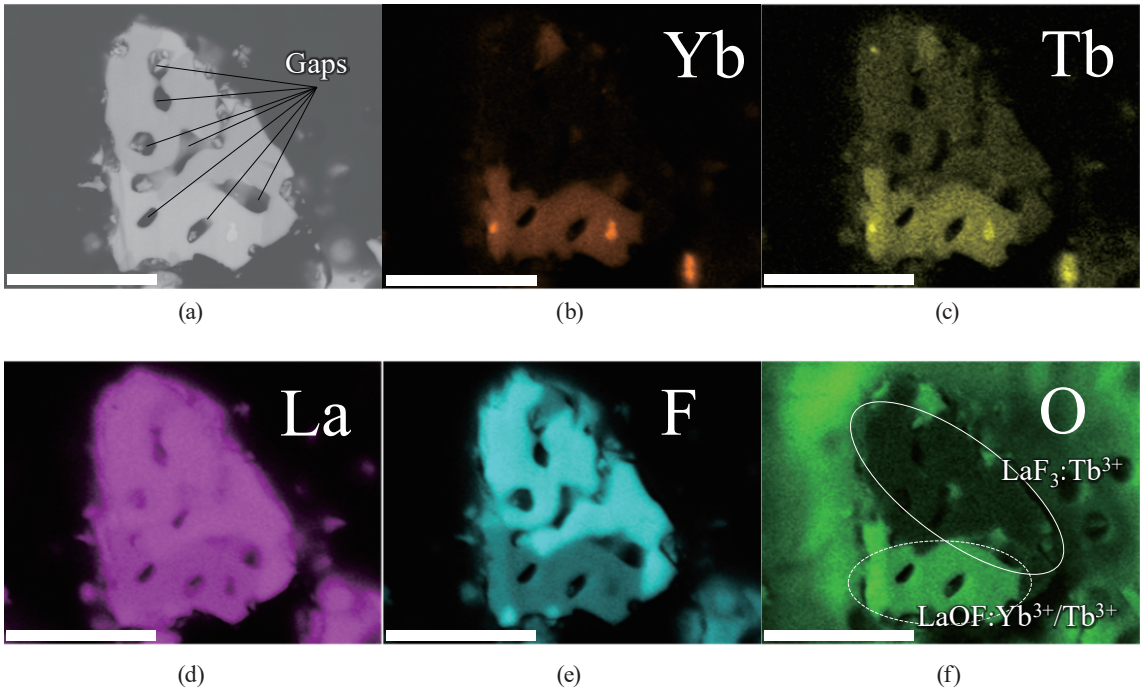

Fig. 3. (Color online) Morphological and elemental analysis results for LaF_3–$LaOF:Yb^{3+}/Tb^{3+}$ with a La:Yb:Tb molar ratio of 1:0.06:0.10. (a) Cross-sectional SEM image and (b)–(f) EDS elemental maps of Yb, Tb, La, F, and O. Scale bar = 10 μm.

image of the sample. The gaps are likely attributed to the partial combination of the particles (LaF_3, Yb_2O_3, and Tb_2O_3) used in the synthesis of LaF_3–LaOF:Yb^{3+}/Tb^{3+}. Furthermore, Figs. 3(b)–3(f) illustrate the EDS elemental mapping of Yb, Tb, La, F, and O, respectively. A thin carbon layer was deposited onto the sample prior to SEM observation; however, its elemental map is not shown. As observed in Figs. 3(d)–3(f), La and F are present throughout the sample. Moreover, regions without [solid line in Fig. 3(f)] and with [dotted line in Fig. 3(f)] abundant O are observed. The crystal structure analysis results in Fig. 2 reveal that the sample is composed of LaF_3 and LaOF; therefore, the regions depicted by the solid and dotted lines in Fig. 3(f) are considered to be composed of LaF_3 and LaOF, respectively. Because the Yb-rich regions overlap with the O-rich regions, Yb is assumed to be mainly doped into LaOF.

The PL analysis results are presented in Fig. 4. The PL spectrum of LaF_3–LaOF:Yb^{3+}/Tb^{3+} possessing a La:Yb:Tb molar ratio of 1:0.06:0.10 depicted in Fig. 4(a) demonstrates peaks at 486

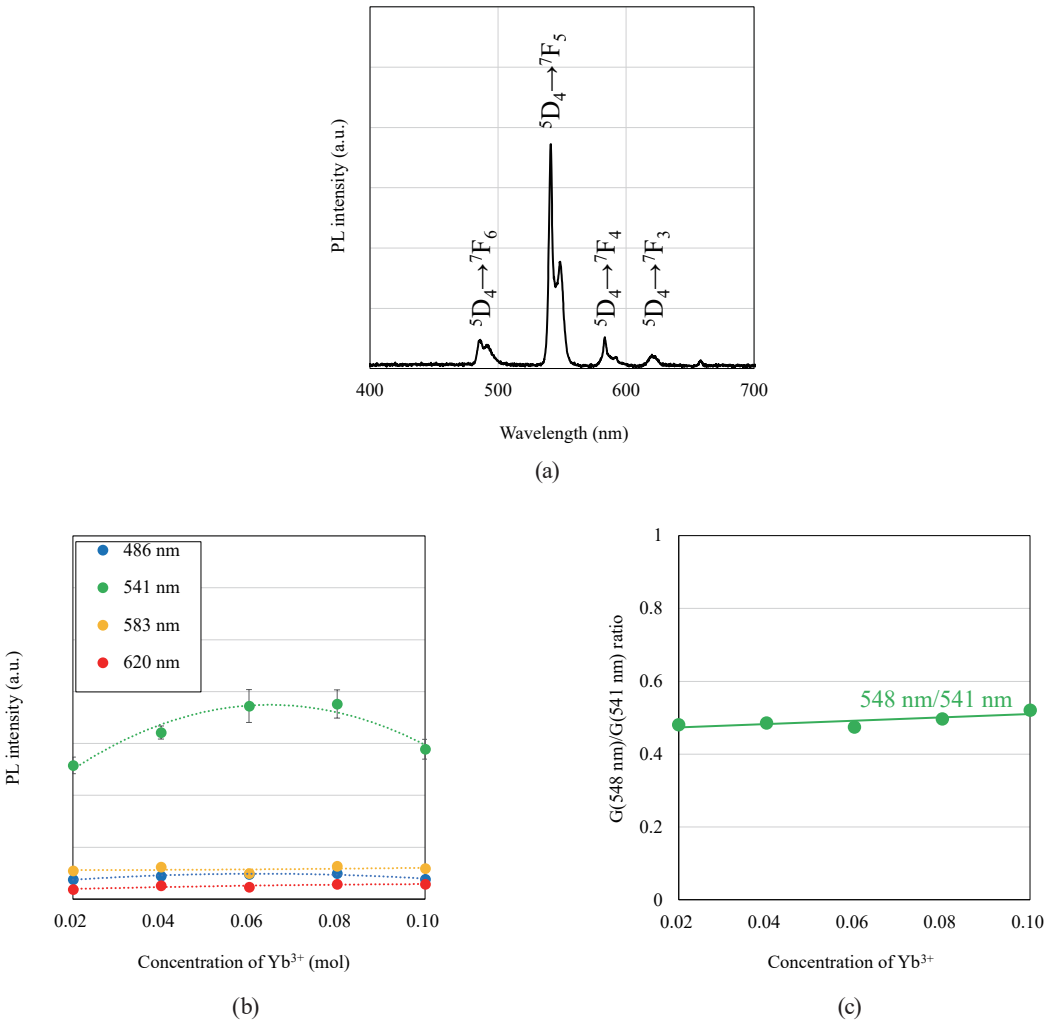

Fig. 4. (Color online) PL analysis results. (a) PL spectrum of LaF_3–LaOF:Yb^{3+}/Tb^{3+} possessing a La:Yb:Tb molar ratio of 1:0.06:0.10. (b) and (c) Yb^{3+} concentration dependence of the PL intensity of LaF_3–LaOF:Yb^{3+}/Tb^{3+} having a La:Yb:Tb molar ratio of 1:x:0.10 (x = 0.02–0.10) and the ratio of the PL intensities at the wavelengths of 541 and 548 nm, respectively. (d) and (e) Tb^{3+} concentration dependence of the PL intensity of LaF3–LaOF:Yb^{3+}/Tb^{3+} possessing a La:Yb:Tb molar ratio of 1:0.06:y (y = 0.08–0.12) and the ratio of the PL intensities at the wavelengths of 541 and 548 nm, respectively.

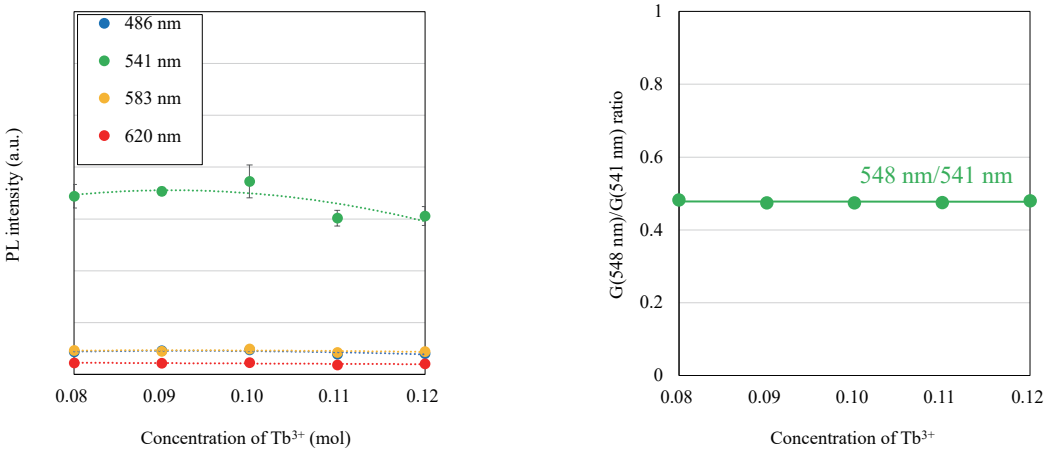

Fig. 4. (Color online) (Continued) PL analysis results. (a) PL spectrum of LaF_3–LaOF:Yb^{3+}/Tb^{3+} possessing a La:Yb:Tb molar ratio of 1:0.06:0.10. (b) and (c) Yb^{3+} concentration dependence of the PL intensity of LaF_3–LaOF:Yb^{3+}/Tb^{3+} having a La:Yb:Tb molar ratio of 1:*x*:0.10 (*x* = 0.02–0.10) and the ratio of the PL intensities at the wavelengths of 541 and 548 nm, respectively. (d) and (e) Tb3+ concentration dependence of the PL intensity of LaF_3–LaOF:Yb^{3+}/Tb^{3+} possessing a La:Yb:Tb molar ratio of 1:0.06:*y* (*y* = 0.08–0.12) and the ratio of the PL intensities at the wavelengths of 541 and 548 nm, respectively.

($^5D_4 \rightarrow {}^7F_6$), 541 ($^5D_4 \rightarrow {}^7F_5$), 583 ($^5D_4 \rightarrow {}^7F_4$), and 620 nm ($^5D_4 \rightarrow {}^7F_3$). In particular, the peak at 541 nm is dominant. Figures 4(b) and 4(c) illustrate the dependence of the PL intensity of LaF_3–LaOF:Yb^{3+}/Tb^{3+} possessing a La:Yb:Tb molar ratio of 1:*x*:0.10 (*x* = 0.02–0.10) on the Yb^{3+} concentration and the ratio of the PL intensities at the wavelengths of 541 and 548 nm, respectively. As observed in Fig. 4(b), the PL intensity of the peak at 541 nm increases for the sample with Yb = 0.06–0.08. The PL intensities of the other peaks are low, rendering the comparisons difficult. As depicted in Fig. 4(c), the ratio of the PL intensities at the wavelengths of 541 and 548 nm is 0.47–0.52. The split peaks at 541 and 548 nm are attributed to the Stark splitting of the $^7F_5$ level.[24]

Figures 4(d) and 4(e) depict the dependence of the PL intensity of LaF_3–LaOF:Yb^{3+}/Tb^{3+} possessing a La:Yb:Tb molar ratio of 1:0.06:*y* (*y* = 0.08–0.12) on the Tb^{3+} concentration and the ratio of the PL intensities at the wavelengths of 541 and 548 nm, respectively. As plotted in Fig. 4(d), the PL intensity increases for the sample featuring Tb = 0.10. The PL intensities of the other peaks are low, rendering the comparisons difficult. Figure 4(e) demonstrates that the ratio of the PL intensities at 541 nm and 548 nm is 0.47–0.48.

Figure 5 shows the pump-power dependence of the PL intensity, which is expressed by the following equation.

$$I_{UC} \propto P^n \tag{1}$$

Here, I_{UC} is the PL intensity, P is the pump power of the excitation source, and n is the number of NIR photons.[25]

Figure 5(a) shows the pump-power dependence of the PL intensity of LaF_3–LaOF:Yb^{3+}/Tb^{3+} possessing a La:Yb:Tb molar ratio of 1:0.06:0.10. Figure 5(b) shows the dependence of the slope

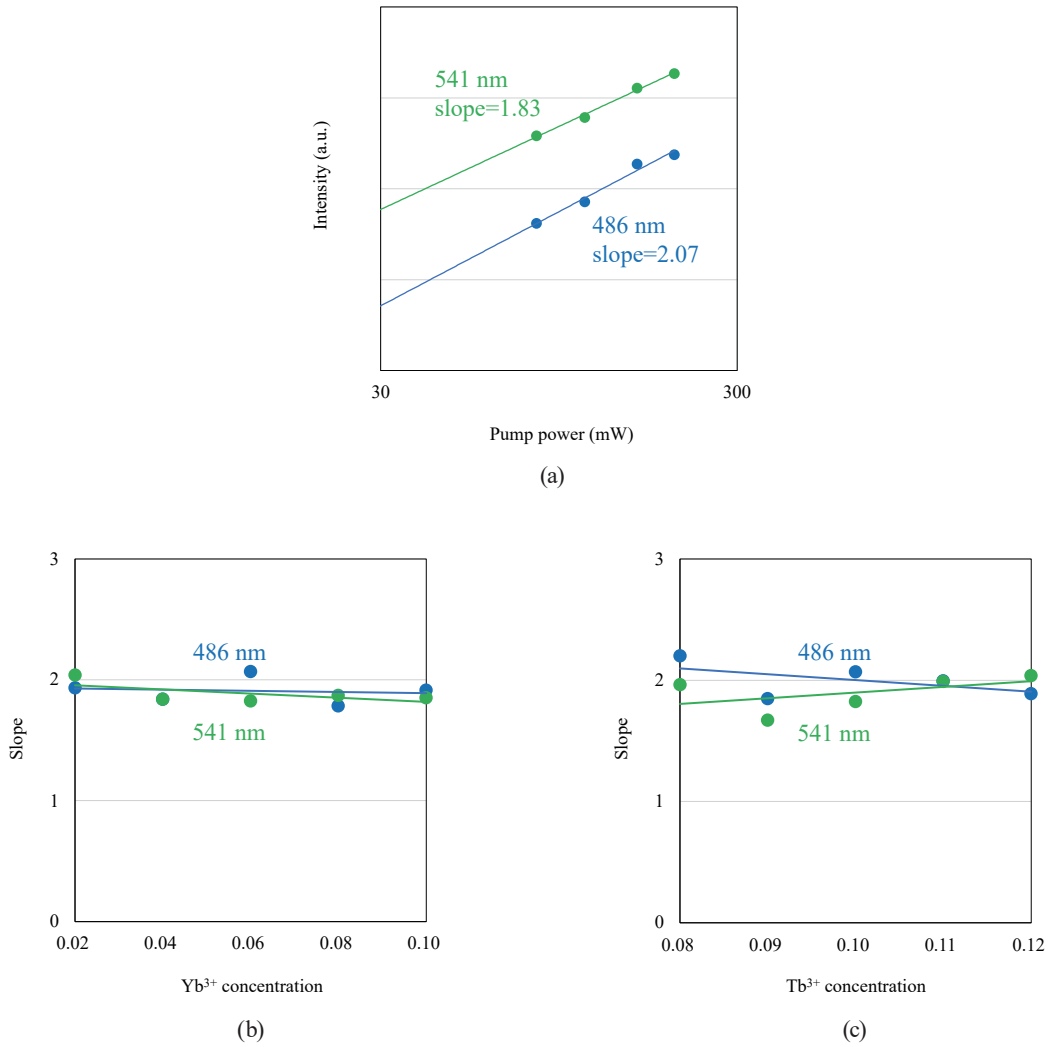

Fig. 5. (Color online) Pump-power dependence of PL intensity. (a) Pump-power dependence of the PL intensity of LaF_3–LaOF:Yb^{3+}/Tb^{3+} possessing a La:Yb:Tb molar ratio of 1:0.06:0.10. (b) Yb^{3+} concentration dependence of the slope of LaF_3–LaOF:Yb^{3+}/Tb^{3+} possessing a La:Yb:Tb molar ratio of 1:x:0.10 (x = 0.02–0.10). (c) Tb^{3+} concentration dependence of the slope of LaF_3–LaOF:Yb^{3+}/Tb^{3+} possessing a La:Yb:Tb molar ratio of 1:0.06:y (y = 0.08–0.12).

of LaF_3–LaOF:Yb^{3+}/Tb^{3+} possessing a La:Yb:Tb molar ratio of 1:x:0.10 (x = 0.02–0.10) on the Yb^{3+} concentration. Figure 5(c) shows the dependence of the slope of LaF_3–LaOF:Yb^{3+}/Tb^{3+} possessing a molar ratio of La:Yb:Tb = 1:0.06:y (y = 0.08–0.12) on the Tb^{3+} concentration. From Fig. 5(a), the slopes of the log–log plots of PL intensity (I_{UC}) versus pump power (P) at 486 nm and 541 nm are 2.07 and 1.83, respectively. Because the slope at each wavelength is approximately equivalent to 2, the emission is a two-photon process. From Fig. 5(b), the slopes at the wavelengths of 486 and 541 nm are 1.79–2.07 and 1.83–2.04, respectively. Figure 5(c) shows that the slopes at the wavelengths of 486 and 541 nm are 1.85–2.20 and 1.67–2.04, respectively.

Figure 6 shows the energy band diagrams for Yb^{3+} and Tb^{3+}. Yb^{3+} ions are excited from the $^2F_{7/2}$ level to the $^2F_{5/2}$ level via stimulation from the light source. The Yb^{3+} ions in the $^2F_{5/2}$ level are subsequently excited to the $^5D_4$ level and undergo cross-relaxation, transferring energy to

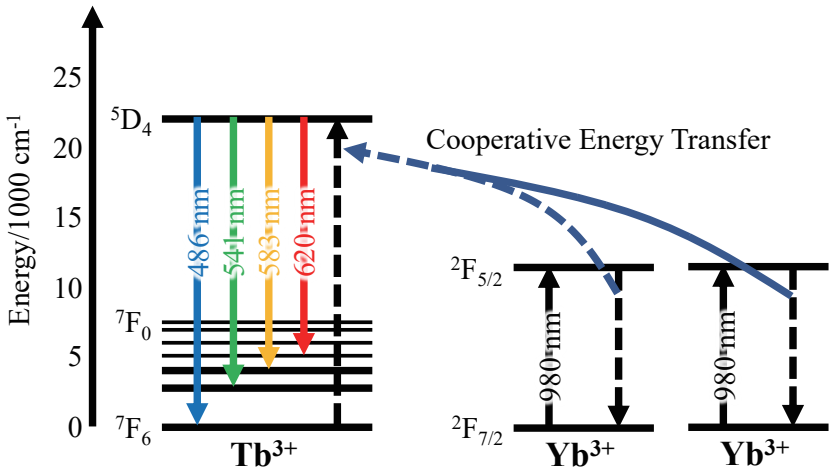

Fig. 6. (Color online) Energy band diagrams for Yb^{3+} and Tb^{3+}.[26]

Tb^{3+} ions. The Tb^{3+} ions in the $^5D_4$ level relax to lower energy levels and emit visible light featuring the wavelengths of 486, 541, 583, and 620 nm.[26]

Because the sample synthesized in this study is a composite of LaF_3 and LaOF, the extent of the contribution of each host material to luminescence is difficult to determine. The elemental mapping results in Fig. 3 indicate that LaOF:Yb^{3+}/Tb^{3+} is luminescent because of the presence of Yb and Tb in the LaOF regions. Conversely, in the LaF_3 regions, Tb is present, whereas the Yb concentration is negligible. Therefore, LaF_3:Tb^{3+} may receive energy from the neighboring LaOF:Yb^{3+}/Tb^{3+} and emit light.

All emission peaks observed in the PL characteristics shown in Fig. 4 originate from the $^5D_4$ level. To calculate the relative sensitivity by the fluorescence intensity ratio method, previous studies suggest that emission peaks from both the $^5D_3$ and $^5D_4$ levels should be observed.[21] Electrons must first acquire energy in the $^5D_4$ level before transitioning to the $^5D_3$ level.[27] To enhance energy transfer efficiency, we plan to incorporate Zn^{2+} to improve luminescence efficiency in future studies.[28]

4. Conclusions

LaF_3–LaOF:Yb^{3+}/Tb^{3+} was synthesized by a solid-state reaction method, and the effects of varying molar ratios on the crystal structure and optical properties were analyzed. Reflectance analysis revealed an absorption peak of Yb^{3+} ($^2F_{7/2}\rightarrow{}^2F_{5/2}$) at a wavelength of approximately 950 nm. Crystal structure analysis via XRD demonstrated that all the synthesized samples were composed of LaOF and LaF_3. Particle analysis via SEM and EDS revealed that some particles were enriched with O, whereas the others were not. PL spectra comprised peaks at 486 ($^5D_4\rightarrow{}^7F_6$), 541 ($^5D_4\rightarrow{}^7F_5$), 583 ($^5D_4\rightarrow{}^7F_4$), and 620 nm ($^5D_4\rightarrow{}^7F_3$), and the peak at 541 nm was particularly dominant. The analysis of the pump-power dependence of the PL intensity demonstrated that the emission was a two-photon process, given that the slopes at the wavelengths of 486 and 541 nm were approximately equivalent to 2.

Conflict of Interest

The authors declare no competing interests.

Acknowledgments

We gratefully acknowledge Professor Toko Sugiura and Professor Takehiko Tsukamoto of the National Institute of Technology, Toyota College (Aichi, Japan), for granting us permission to use their experimental facilities. This work was supported by JSPS KAKENHI (grant number 23K13377).

References

1 F. Auzel: Chem. Rev. **104** (2004) 139. https://doi.org/10.1021/cr020357g
2 F. Auzel: C. R. Acad. Sci. Paris **262** (1966) 1016. https://cir.nii.ac.jp/crid/1573950399692310784
3 F. Auzel: J. Lumin. **223** (2020) 116900. https://doi.org/10.1016/j.jlumin.2019.116900
4 H. S. Mader, P. Kele, S. M. Saleh, and O. S. Wolfbeis: Curr. Opin. Chem. Biol. **14** (2010) 582. https://doi.org/10.1016/j.cbpa.2010.08.014
5 E. M. Mettenbrink, W. Yang, and S. Wilhelm: Adv. Photonics Res. **3** (2022) 2200098. https://doi.org/10.1002/adpr.202200098
6 W. Yang, X. Li, D. Chi, H. Zhang, and X. Liu: Nanotech. **25** (2014) 482001. https://doi.org/10.1088/0957-4484/25/48/482001
7 A. A. Ansari and M. Sillanpää: Renew. Sustain. Energy Rev. **151** (2021) 111631. https://doi.org/10.1016/j.rser.2021.111631
8 R. K. Jain, S. N. Ananya, P. J. Anand, and D. Sunil: Microchem. J. **209** (2025) 112749. https://doi.org/10.1016/j.microc.2025.112749
9 Y. Zhao, X. Wang, Y. Zhang, Y. Li, and X. Yao: J. Alloy. Compd. **817** (2020) 152691. https://doi.org/10.1016/j.jallcom.2019.152691
10 H. Suo, X. Zhao, Z. Zhang, Y. Wang, J. Sun, M. Jin, and C. Guo: Laser Photonics Rev. **15** (2021) 2000319. https://doi.org/10.1002/lpor.202000319
11 F. Li, L. Tu, Y. Zhang, D. Huang, X. Liu, X. Zhang, J. Du, R. Fan, C. Yang, K. W. Krämer, J. Marques-Hueso, and G. Chen: Nat. Photonics **18** (2024) 440. https://doi.org/10.1038/s41566-024-01393-3
12 J. F. Suyver, J. Grimm, M. K. van Veen, D. Biner, K. W. Krämer, and H. U. Güdel: J. Lumin. **117** (2006) 1. https://doi.org/10.1016/j.jlumin.2005.03.011
13 F. Wang and X. Liu: J. Am. Chem. Soc. **130** (2008) 5642. https://doi.org/10.1021/ja800868a
14 J. J. Velázquez, V. D. Rodríguez, A. C. Yanes, J. del-Castillo, and J. Méndez-Ramos: Opt. Mater. **34** (2012) 1994. https://doi.org/10.1016/j.optmat.2011.12.020
15 X. Cheng, X. Ma, H. Zhang, Y. Ren, and K. Zhu: Phys. B Condens. Matter. **521** (2017) 270. https://doi.org/10.1016/j.physb.2017.07.011
16 T. Nonaka, Y. Inoue, M. Yamamoto, and S.-I. Yamamoto: Braz. J. Phys. **55** (2025) 24. https://doi.org/10.1007/s13538-024-01665-x
17 T. Nonaka, T. Sugiura, T. Tsukamoto, and S.-I. Yamamoto: J. Korean Ceram. Soc. **59** (2022) 889. https://doi.org/10.1007/s43207-022-00231-y
18 J. Li, X. Zhou, J. Ding, X. Zhou, and Y. Wang: J. Mater. Chem. C **7** (2019) 2257. https://doi.org/10.1039/C8TC05330H
19 Y. Wei, J. Li, J. W. Yang, X. N. Chi, and H. Guo: J. Lumin. **137** (2013) 70. https://doi.org/10.1016/j.jlumin.2012.11.017
20 P. Deshmukh, R.K. Deo, A. Ahlawat, A. A. Khan, R. Singh, A. K. Karnal, and S. Satapathly: J. Alloy. Compd. **859** (2021) 157857. https://doi.org/10.1016/j.jallcom.2020.157857
21 D. E. T. dos Santos, A. Torquato, I. V. Barbosa, J. F. Carvalho, L. J. Q. Maia, and R. C. D. Santana: J. Alloy. Compd. **1010** (2025) 177444. https://doi.org/10.1016/j.jallcom.2024.177444
22 D. Avram, I. Porosnicu, B. Cojocaru, M. Florea, and C. Tiseanu: J. Lumin. **179** (2016) 265. https://doi.org/10.1016/j.jlumin.2016.07.026

23 R. D. Shannon: Acta Cryst. A**32** (1976) 751. https://doi.org/10.1107/S0567739476001551
24 N. B. Amar, M. A. Hassairi, and M. Dammak: J. Lumin. **173** (2016) 223. https://doi.org/10.1016/j.jlumin.2016.01.023
25 S. Tamboli, G. B. Nair, A. K. Sharma, S. J. Dhoble, and H. C. Swart: Mater. Res. Bull. **169** (2024) 112503. https://doi.org/10.1016/j.materresbull.2023.112503
26 D. Li, H. Liao, Q. Zhang, Q. Fan, and J. She: Microchem. J. **203** (2024) 110947. https://doi.org/10.1016/j.microc.2024.110947
27 T. Grzyb, K. Kubasiewicz, A. Szczeszak, and S. Lis: J. Alloy. Compd. **686** (2016) 951. https://doi.org/10.1016/j.jallcom.2016.06.230
28 M. I. Sarkar, K. Shwetabh, M. S. Singh, and K. Kumar: Sens. Actuators, A **386** (2025) 116329. https://doi.org/10.1016/j.sna.2025.116329